nanomaterials

MDPI

Article

Thermal Analysis of Metal-Organic Precursors for Functional Cu:NiO_x Hole Transporting Layer in Inverted Perovskite Solar Cells: Role of Solution Combustion Chemistry in Cu:NiO_x Thin Films Processing

Apostolos Ioakeimidis [1], Ioannis T. Papadas [1,2], Eirini D. Koutsouroubi [3], Gerasimos S. Armatas [3] and Stelios A. Choulis [1,*]

[1] Molecular Electronics and Photonics Research Unit, Department of Mechanical Engineering and Materials Science and Engineering, Cyprus University of Technology, Limassol 3036, Cyprus; a.ioakeimidis@cut.ac.cy (A.I.); ioannis.papadas@cut.ac.cy (I.T.P.)
[2] Department of Public and Community Health, School of Public Health, University of West Attica, 11521 Athens, Greece
[3] Department of Materials Science and Technology, University of Crete, 70013 Heraklion, Greece; eirinink@materials.uoc.gr (E.D.K.); garmatas@materials.uoc.gr (G.S.A.)
* Correspondence: stelios.choulis@cut.ac.cy

check for updates

Citation: Ioakeimidis, A.; Papadas, I.T.; Koutsouroubi, E.D.; Armatas, G.S.; Choulis, S.A. Thermal Analysis of Metal-Organic Precursors for Functional Cu:NiO_x Hole Transporting Layer in Inverted Perovskite Solar Cells: Role of Solution Combustion Chemistry in Cu:NiO_x Thin Films Processing. *Nanomaterials* **2021**, *11*, 3074. https://doi.org/10.3390/nano11113074

Academic Editors: Jingjing Chang and Seok-In Na

Received: 8 October 2021
Accepted: 12 November 2021
Published: 15 November 2021

Publisher's Note: MDPI stays neutral with regard to jurisdictional claims in published maps and institutional affiliations.

Abstract: Low temperature solution combustion synthesis emerges as a facile method for the synthesis of functional metal oxides thin films for electronic applications. We study the solution combustion synthesis process of Cu:NiO_x using different molar ratios (w/o, 0.1 and 1.5) of fuel acetylacetone (Acac) to oxidizer (Cu, Ni Nitrates) as a function of thermal annealing temperatures 150, 200, and 300 °C. The solution combustion synthesis process, in both thin films and bulk Cu:NiO_x, is investigated. Thermal analysis studies using TGA and DTA reveal that the Cu:NiO_x thin films show a more gradual mass loss while the bulk Cu:NiO_x exhibits a distinct combustion process. The thin films can crystallize to Cu:NiO_x at an annealing temperature of 300 °C, irrespective of the Acac/Oxidizer ratio, whereas lower annealing temperatures (150 and 200 °C) produce amorphous materials. A detail characterization study of solution combustion synthesized Cu:NiO_x, including XPS, UV-Vis, AFM, and Contact angle measurements, is presented. Finally, 50 nm Cu:NiO_x thin films are introduced as HTLs within the inverted perovskite solar cell device architecture. The Cu:NiO_x HTL annealed at 150 and 200 °C provided PVSCs with limited functionality, whereas efficient triple-cation $Cs_{0.04}(MA_{0.17}FA_{0.83})_{0.96}$ $Pb(I_{0.83}Br_{0.17})_3$-based PVSCs achieved for Cu:NiO_x HTLs for annealing temperature of 300 °C.

Keywords: Cu:NiO_x; metal oxides; solution combustion synthesis; metal-organic precursors; fuels; oxidizers; electronic thin films; hole transporting layers; annealing temperature; perovskite solar cells

1. Introduction

Perovskite solar cells (PVSCs) have witnessed significant progress related to power conversion efficiency within the last decade, climbing from 3.8% in 2009 to more than 24% in the year 2021 for single junction cells [1,2]. Some of the most promising hole transporting layers (HTLs) for inverted PVSCs are thin films of pristine or doped NiO_x materials grown with various deposition methods. Thanks to its p-type semiconducting nature, high optical transmittance, enhanced electrical conductivity, and deep-lying valence band (VB) that matches well with the VB of hybrid perovskite photoactive layer, NiO_x emerges as an excellent hole transporting layer (HTL) material for inverted perovskite solar cells [3–16]. Doping of NiO_x with Copper (Cu) has been shown to improve the conductivity and charge collection properties, resulting in higher PCE-inverted perovskite solar cells. Jong H. Kim studied the performance of PEDOT:PSS, NiO_x, and 5% Cu doped NiO_x (Cu:NiO_x) HTLs

relevant to the performance of inverted perovskite photovoltaic. Among them, Cu:NiO_x exhibited the highest PCE (14.89%) due to having a better valence band (VB) alignment with the perovskite active layer compared to PEDOT:PSS HTL, while, in comparison to pristine NiO_x, the higher PCE was ascribed to increased Cu:NiO_x electrical conductivity (8.4×10^{-4} S.cm^{-1}) due to Cu doping [17]. Wei Chen et al. has reported that doping of NiO_x with 5% Cu induces a slight downshift of VB from 5.16 to 5.25 eV and at the same time increases both carrier concentration and hole mobility of the Cu:NiO_x HTL. The Cu:NiO_x HTL-based inverted perovskite solar cells provided an increased PCE of 18.01% compared to pristine NiO_x HTL-based solar cells (16.68%), retaining 95% of the PCE after 1000 h storage in air [18]. However, NiO_x HTL derivatives prepared by sol-gel method usually need to be annealed at relatively high temperatures (over 400 °C) in order to achieve high crystallinity [19–22]. Sol-gel reactions are endothermic, and thus require high external thermal energy to form metal oxide lattices and remove organic residuals [23–26]. This high processing temperature increases the cost of device fabrication and also inhibits the implementation of printing manufacturing for producing next generation solution-processed photovoltaics on conventional flexible substrates.

Combustion synthesis methods have been reported by many researchers as a beneficial route of the synthesis of high crystalline metal oxides at lower temperatures than those used for sol-gel reactions. The combustion process's exothermic reaction provides a lower transition energy with which to form the metal oxide crystal lattices, avoiding the need for high thermal energy. Thus, the solution combustion synthesis (SCS) method is being adopted for the synthesis of metal oxides electronic thin films due to its cost-effectiveness, simplicity, enhanced electronic material functionality, and relatively lower required processing annealing temperatures [27–35].

Over the last years, there have been many reports on the use of solution combustion synthesis of metal oxide such as Cu:CrO_x and ZnO for charge transporting layers in perovskite solar cells and Amorphous Indium Gallium Zinc oxide (IGZO) for metal oxide thin film transistors applications [28,30,36,37]. We have reported the solution combustions synthesis of pristine and co-doped (Cu, Li) $NiCo_2O_4$ films, applying a 300 °C annealing temperature and incorporating them as high performance HTLs in $MAPbI_3$-based inverted perovskite solar cells [38,39]. We have also shown the improvements of PVSC's thermal stability based on SCS Cu:NiO_x HTL by treatment of Cu:NiO_x with β-alanine, showing a T80 of 1000 h under heat conditions (60 °C, N_2), as well as the improvement of humidity degradation resistance for SCS NiO_x-based PVSC with the addition of 1% Nitrobenzene within the perovskite active layer [40,41]. Jae Woong Jung et al. have reported the solution combustion synthesis of the Cu:NiO_x film at 150 °C and implemented it as HTL in $MAPbI_3$ perovskite solar cell. They showed that the combustion-synthesized Cu:NiO_x resulted in better power conversion efficiency (PCE) for perovskite solar cells compare to devices containing a typical sol-gel synthesized Cu:NiO_x HTL [42]. Other reports on the solution combustion synthesis of pristine and doped NiO_x have applied a range of annealing temperatures for the fabrication of HTLs for efficient perovskite solar cells [43–48]. For example, Ziye Liu et al. reported that the fabrication of an $MA_{1-y}FA_yPbI_{3-x}Cl_x$ perovskite solar cell using solution combustion synthesized NiO_x, achieving a high PCE of more than 20%. The applied temperature of the NiO_x solution combustion synthesis for high efficiency devices was 250 °C while, for a 150 °C annealing temperature, the devices exhibited a rapid deterioration of their PCE [46]. Ao Liu et al. demonstrated the solution combustion synthesis fabrication of optimized 5% Cu doped NiO_x films for use in TFT applications, exhibiting excellent electrical performance [49]. Yi-Huan Li et al. applied a 300 °C annealing temperature for the solution combustion synthesis of Cu:NiO_x, showing that it can be used as an efficient hole injection layer for the fabrication of high performing OLEDs [50]. Thus, solution combustion synthesis metal oxide thin films have emerged as a facile method for the fabrication of functional metal oxide-based charge selective contacts for electronic applications. Nevertheless, there have been reports that the combustion synthesis of thin electronic films differ from the corresponding bulk analogues, and thus

a low annealing temperature combustion synthesis of thin films cannot be deduced by the bulk material behavior, even suggesting that low temperature combustion synthesis is unlikely to occur during the processing of thin film precursors [51–56]. Thus, the processing annealing conditions for the solution combustion synthesis of functional Cu:NiO_x HTLs needs further investigation.

The aim of this paper is to identify the Cu:NiO_x HTL annealing processing conditions and to examine the fuel to oxidizer ratio for efficient inverted PVSCs. We study in detail the Cu:NiO_x thin films solution combustion synthesis process as a common metal oxides HTL that is widely used in inverted perovskite solar cells. Specifically, the reported results investigate the effect of the thermal annealing temperature (150, 200, and 300 °C) as well as the fuel (acetyl acetonate (Acac)) to oxidizer (Cu and Ni nitrates) ratio (without (w/o), 0.1 and 1.5) in the combustion synthesis process of Cu:NiO_x. The study is performed at Cu:NiO_x filmswith various final thicknesses (50, 200, 300 nm) and for drop-casted bulk Cu:NiO_x analogues (with thickness in the range of a few microns). The crystal growth process is studied by performing thermogravimetric analysis (TGA) and the crystallinity of the corresponding Cu:NiO_x materials is examined by X-ray diffraction (XRD). Furthermore, we characterized the thin Cu:NiO_x film properties processed under the above-mentioned conditions using XPS, contact angle, AFM, and UV-Vis spectroscopy techniques. Finally, we evaluated the impact of SCS-based Cu:NiO_x thin film properties on the PCE performance of inverted PVSCs containing Cu:NiO_x HTL and the triple cation perovskite [$Cs_{0.04}(MA_{0.17}FA_{0.83})_{0.96}Pb(I_{0.83}Br_{0.17})_3$] as a photoactive layer.

2. Materials and Methods

Materials: Prepatterned glass-ITO substrates (sheet resistance 4 Ω/sq) were purchased from Psiotec Ltd., Berkhamsted, UK. All the other chemicals used in this study were purchased from Sigma Aldrich (St. Louis, MO, USA).

Cu:NiO_x solution combustion synthesis: In a typical synthesis, 0.95 mmol $Ni(NO_3)_2.6H_2O$ and 0.05 mmol $Cu(NO_3)_2.3H_2O$ were dissolved in 10 mL 2-methoxyethanol with different concentrations of fuel acetylacetonate to the solution and the mixture was further stirred for 1 h at room temperature. Then, the samples were dried at 80 °C for 5 min and annealed at 150 °C, 200 °C, or 300 °C in air for 1 h. The chemical reaction formula of the solution combustion synthesis is as follows:

$$Ni(NO_3)_2{\cdot}6H_2O + Cu(NO_3)_2{\cdot}3H_2O + C_5H_8O_2 \Rightarrow Cu{:}NiO_x\ (s) + \uparrow H_2O + \uparrow CO_2 + \uparrow N_2$$

Samples preparations for TGA, AFM, UV-Vis, contact angle analysis: For the thermogravimetric analysis (TGA) of the combustion synthesis behavior of the Cu:NiO_x films, the samples were fabricated onto Alumina disk substrates by blade-coating in air. For the AFM, UV-Vis, and contact angle measurements, the Cu:NiO_x films were fabricated by doctor blade on quartz substrates.

Device fabrication: ITO-patterned glass substrates were cleaned using an ultrasonic bath for 10 min in acetone followed by 10 min in isopropanol. The Cu:NiO_x precursors were prepared and blade-coated on ITO substrates as described in the Cu:NiO_x solution combustion synthesis section. For the preparations of the triple cation $Cs_{0.04}(MA_{0.17}FA_{0.83})_{0.96}Pb(I_{0.83}Br_{0.17})_3$ perovskite solutions, a previous reported method was used [57]. The perovskite films were fabricated on top of Cu:NiO_x inside a N_2 atmosphere glovebox by spin-coating at 5000 rpm for 35 s and after 10 s. 300 mL of ethyl acetate were dropped onto the spinning substrate as the anti-solvent to achieve the rapid crystallization of the films. The resulting perovskite films were annealed at 100 °C for 60 min. For the electron transporting layers, a $PC_{60}BM$ film was coated on top of perovskite inside the glovebox using spin coating at 1000 rpm for 30 s from a 20 mg/mL chlorobenzene solution. To complete the devices, 7 nm of bathocuproine (BCP) was thermally evaporated followed by 80 nm of Ag. The schematic illustration of the SCS-based Cu:NiO_x HTL and PVSC fabrication process and the corresponding device structure are presented in Figure 1.

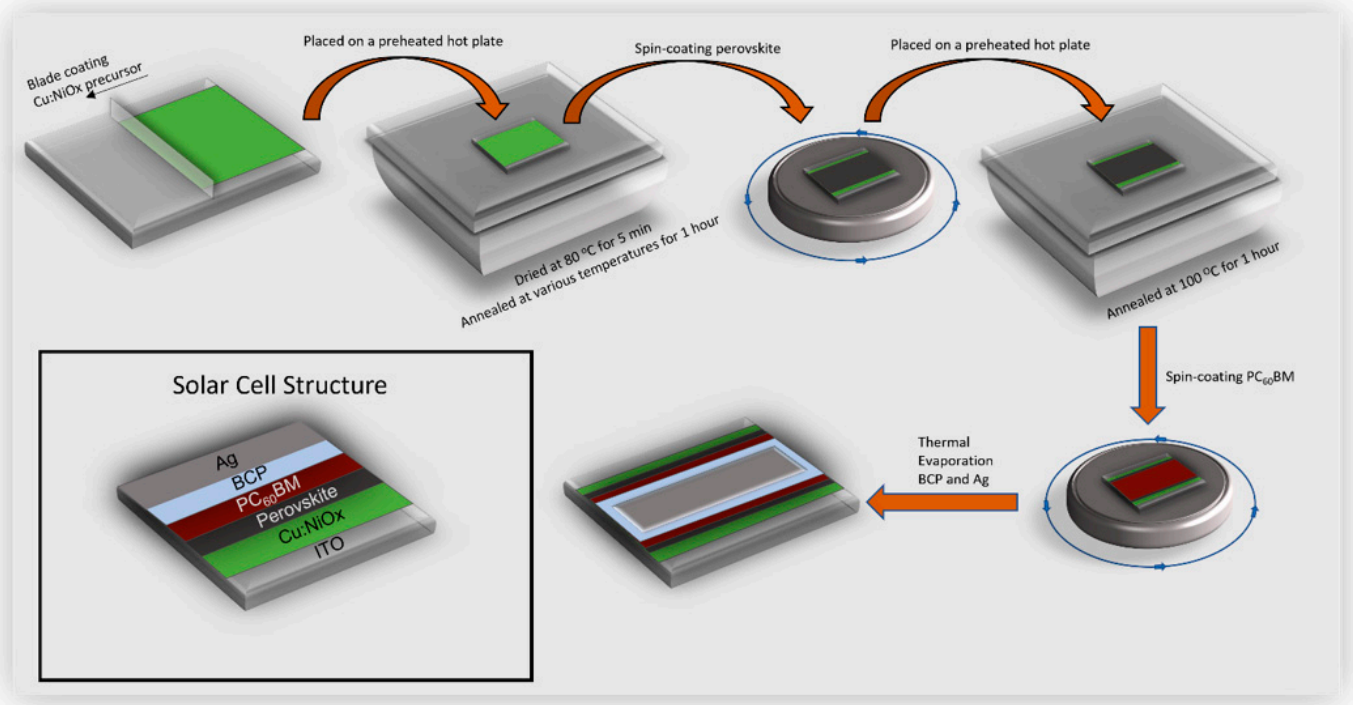

Figure 1. Schematic illustration of SCS based Cu:NiO_x HTL and perovskite device fabrication process and the layer structuring.

Characterization: Thermogravimetric analysis (TGA) and differential thermal analysis (DTA) was performed on a Shimadzu. Samples were heated up to 400 °C in air atmosphere (200 mL min^{-1} flow rate) with a heating rate of 10 °C min^{-1} and alumina (Al_2O_3), a substance with the same thermal mass as the sample, was used for reference material analysis. Powder X-ray diffraction (XRD) patterns were recorded on a PANalytical X'Pert Pro X-ray diffractometer with a Ni-filtered Cu Kα source (λ = 1.5418 Å), operating at 45 kV and 40 mA. X-ray photoelectron spectroscopy (XPS) analysis conducted on a SPECS spectrometer using a Phoibos 100 1D-DLD electron analyzer and an Al Kα radiation as the energy source (1486.6 eV). Binding energy values were corrected for charging by assigning a bending energy of 284.8 eV to the C 1 s signal of adventitious carbon. For UV-Vis absorption and atomic force microscopy (AFM) measurements, the films were fabricated on quartz substrates. UV-Vis absorption measurements were performed with a Schimadzu UV-2700 UV-Vis spectrophotometer. AFM images were obtained using a Nanosurf easy scan 2 controller applying tapping mode. The thickness of the films was measured with a Veeco Dektak 150 profilometer. Contact angle (CA) measurements were performed using a KRUSS DSA 100E drop analysis system. The current density–voltage (J/V) characteristics were characterized with a Botest LIV Functionality Test System. For illumination, a calibrated Newport Solar simulator equipped with an Xe lamp was used, providing an AM1.5G spectrum at 100 mW/cm^2, as measured by a certified oriel 91150V calibration cell. A shadow mask was attached to each device prior to measurements to accurately define 0.09 cm^2 device area.

3. Results

3.1. TGA Results of Cu:NiO_x (Films versus Bulk Precursors)

The synthesis behavior of the Cu:NiO_x thin films and corresponding bulk mixtures onto alumina disc substrates was examined through thermogravimetric analysis (TGA) and differential thermal analysis (DTA). Figure 2a,b presents the TGA and the corresponding DTA curves of the 50 nm thick Cu:NiO_x films prepared with a different molar ratio of fuel (Acac) to oxidizer (Cu and Ni nitrates), namely without (w/o) Acac, 0.1 and 1.5, and drying the films at 80 °C. The Cu:NiO_x film w/o Acac shows a mass loss near ~130 °C,

indicating the thermal instability of this precursor in the absence of any fuel additive. For the Cu:NiO_x films prepared with 0.1 and 1.5 Acac/oxidizer molar ratio, the TGA profiles show similar thermal decomposition behavior, exhibiting a gradual mass loss after T > ignition temperature (T_{ig}). This is inconsistent with a combustion process that occurs to the combustible precursors, as is be shown below. Near 300 °C, the TGA profiles for all samples display an intense mass loss, which is associated with an exothermic peak on the DTA curve. This is attributed to the decomposition of metal complexes and the crystallization of the Cu:NiO_x oxide. Thus, films present two stages of mass loss, at ~130 °C and ~300 °C for drying at 80 °C irrespective of Acac addition in precursor solution. The corresponding DTA results are presented in Figure 2b. For the sample w/o Acac, an negligible broad exothermic peak is observed at ~130 °C and another broad exotherm peak around ~300 °C. For the samples containing 0.1 and 1.5 Acac, low intensity, abrupt exothermic peaks are observed at ~130 °C and broad exothermic peaks around ~300 °C. Thus, the addition of Acac in the precursor induces a limited combustion process by reacting with a part of the oxidizer at ~130 °C, facilitating the removal of the organic residuals.

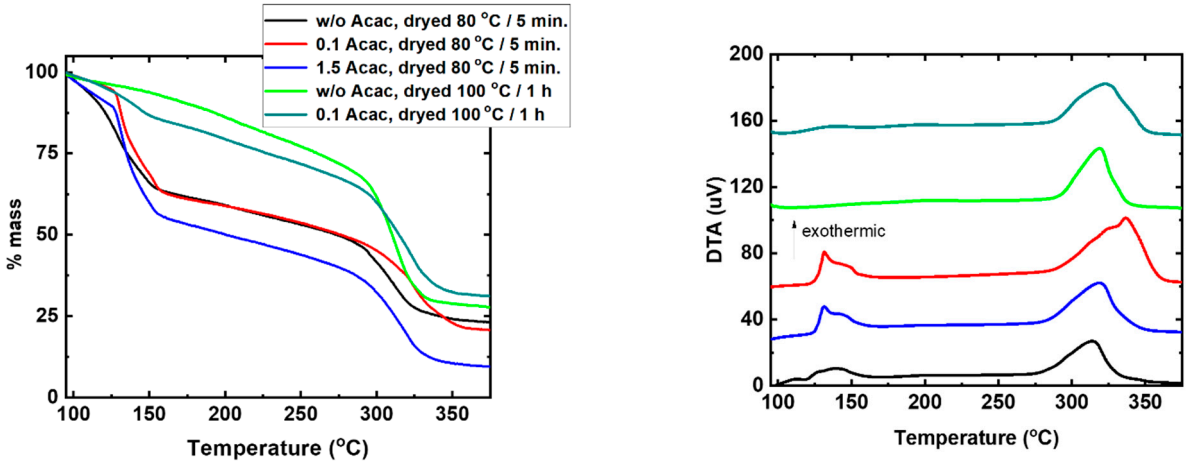

(**a**) (**b**)

Figure 2. (**a**) TGA curves of precursor films without (w/o) fuel and containing 0.1 and 1.5 molar ratio of fuel (Acac) to oxidizer (Cu, Ni nitrates) in 2-methoxy ethanol dried at 80 and 100 °C, and (**b**) the respective DTA curves.

The mass loss at ~130 °C of the sample w/o Acac suggests that the 2-methoxy ethanol, except for its role as a solvent, could also behave as a fuel. To support this, higher drying temperature (100 °C) for 1 h was applied to the film's synthesis, where most of 2-methoxy ethanol was evaporated. In this case, the TGA curve showed no mass loss and the corresponding DTA curve exhibited analogous behavior without any endothermic or exothermic reaction at 130 °C, while, for the film prepared with a Acac/oxidizer molar ratio of 0.1, a marginal mass loss occurred during the first stage of combustion (at ~130 °C). This means that the films that require non-combustive Cu:NiO_x precursors require high temperatures of over 300 °C for the complete conversion of the precursors into the metal oxide lattice.

Further, we compared the combustion synthesis behavior of Cu:NiO_x thin films (50, 200, 300 nm) and bulk analogues (thickness range of a few microns). TGA profiles (Figure 3a) show that, by increasing the thickness of the film, a more intense gradual mass loss occurs at ~130 °C, with the second mass loss at ~300 °C becoming less prominent, while comparatively full combustion could occur at bulk materials at ~130 °C. Thus, we can infer that the mass of the precursor has a significant impact on the complete combustion synthesis reactions. The DTA results, in Figure 3c, are in accordance with the TGA profile, where the raise of thickness in Cu:NiO_x precursors layers shows a more intense exothermic peak at 130 °C; this corresponds to almost complete mass loss, gradually decreasing the exothermic peak at around 300 °C. Additionally, the absence of fuel (Acac) and the impact

of solvent was examined once again during the combustion process for bulk materials. As observed in TGA profile (Figure 3b), a rapid mass loss occurs at ~130 °C w/o Acac for samples dried at 80 and 100 °C for 5 min, respectively. The corresponding DTA curves (Figure 3d) show a single sharp exotherms at ~130 °C that corresponds exactly to the abrupt mass loss in the TGA (Figure 3b); this process is sufficient to lead the reaction rapidly to completion for metallic Ni formation as will be shown in XRD analysis below. In contrast, in the preheated sample at 100 °C for an extended period (48 h), where most of the solvent was evaporated, combustion reaction could not occur. This sample exhibits only an intense exothermic peak of around ~300 °C, which corresponds to the crystal phase formation of NiO. These observations are in agreement with previous reports that the organic solvent 2-methoxy ethanol plays a dual role of acting both as a solvent and also as a fuel in addition to Acac for the formation of the metal oxide lattices by the solution combustion synthesis [58].

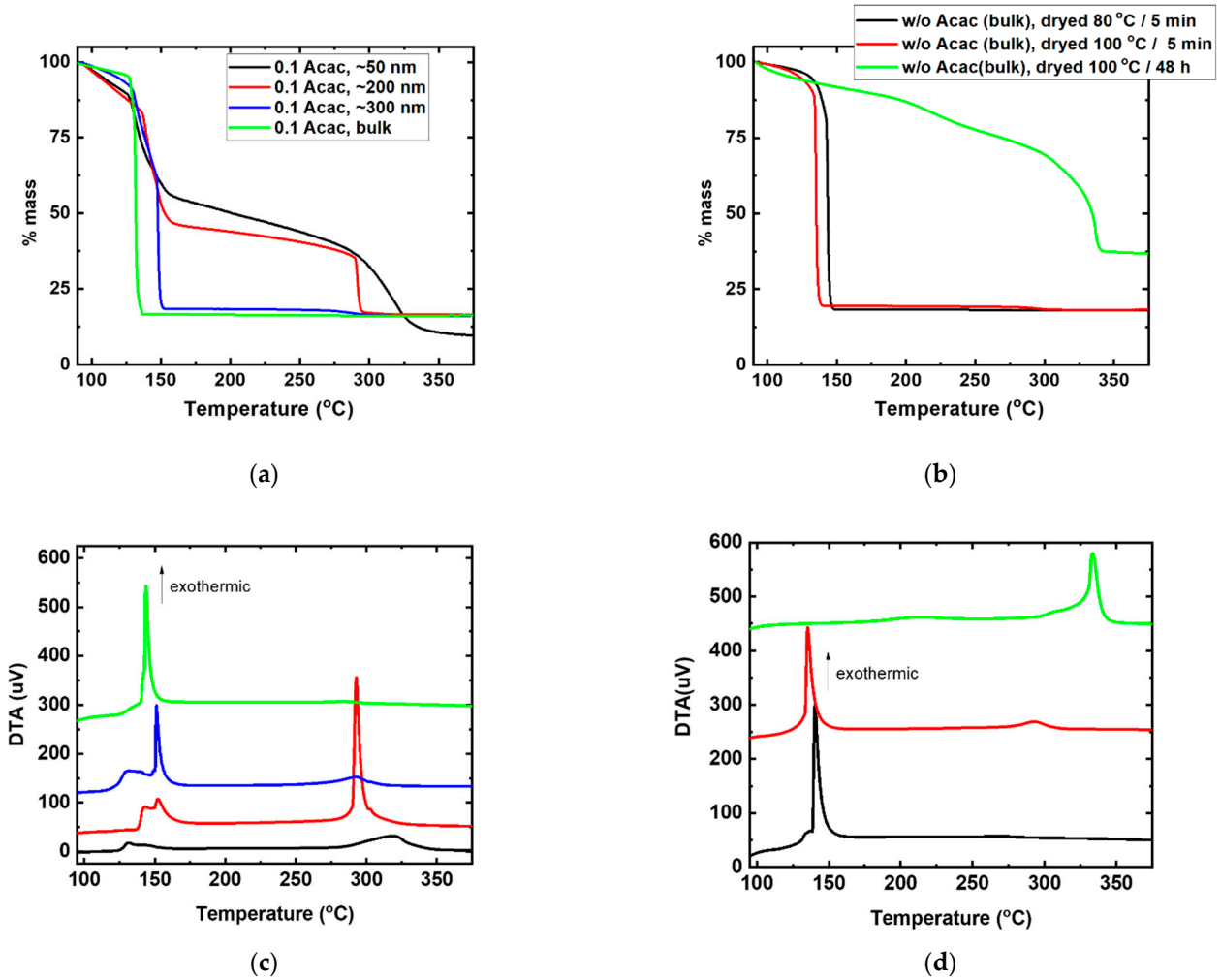

Figure 3. (**a**) TGA curves of different thickness (50, 200, 300 nm and bulk) films containing 0.1 molar ratio of fuel (Acac) to oxidizer (Cu, Ni nitrates) in 2-methoxy ethanol and (**b**) TGA curves of combustion-synthesized bulk samples prepared from precursor with Cu and Ni nitrates but without (w/o) Acac and 2-methoxy ethanol as solvent dried at 80 °C and 100 °C for 5 min and at 100 °C for 48 h. The respective DTA curves for (**c**) different thickness (50, 200, 300 nm and bulk) and (**d**) bulk samples.

3.2. XRD Results of Cu:NiO_x Films and Bulk Precursors

The crystallinity of the SCS Cu:NiO_x thin films (identical to the Cu:NiO_x HTLs that were used within the inverted PVSCs) was examined using X-ray diffraction (XRD) analysis. Figure 4a–c presents the XRD patterns of the films prepared using w/o, 0.1, and 1.5 Acac

and annealing temperatures of 150, 200, and 300 °C. The crystal phase of NiO can be obtained for an annealing temperature of 300 °C regardless of the containing amount of Acac, while, for 150 and 200 °C, no crystal phase was detected. For the 300 °C annealing temperature, the characteristic diffraction peaks of NiO appeared at 2θ = 37.20°, 43.0°, 62.87°, and 75.20°, which can be indexed to the cubic crystal structure of NiO as (111), (200), (220), and (311) planes, respectively (JCPDS No. 01-089-5881). For the film containing 1.5 Acac and annealed at 300 °C, the formation of mixed crystal phases of NiO and metallic Ni was observed. Specifically, XRD patterns, along with the NiO diffractions, reveal additional peaks at 2θ = 44.0°, 52.3°, and 76.5° assigned to (111), (200), and (220) planes, respectively, of the face-centered cubic (FCC) phase of Ni (JCPDS No. 87-0712).

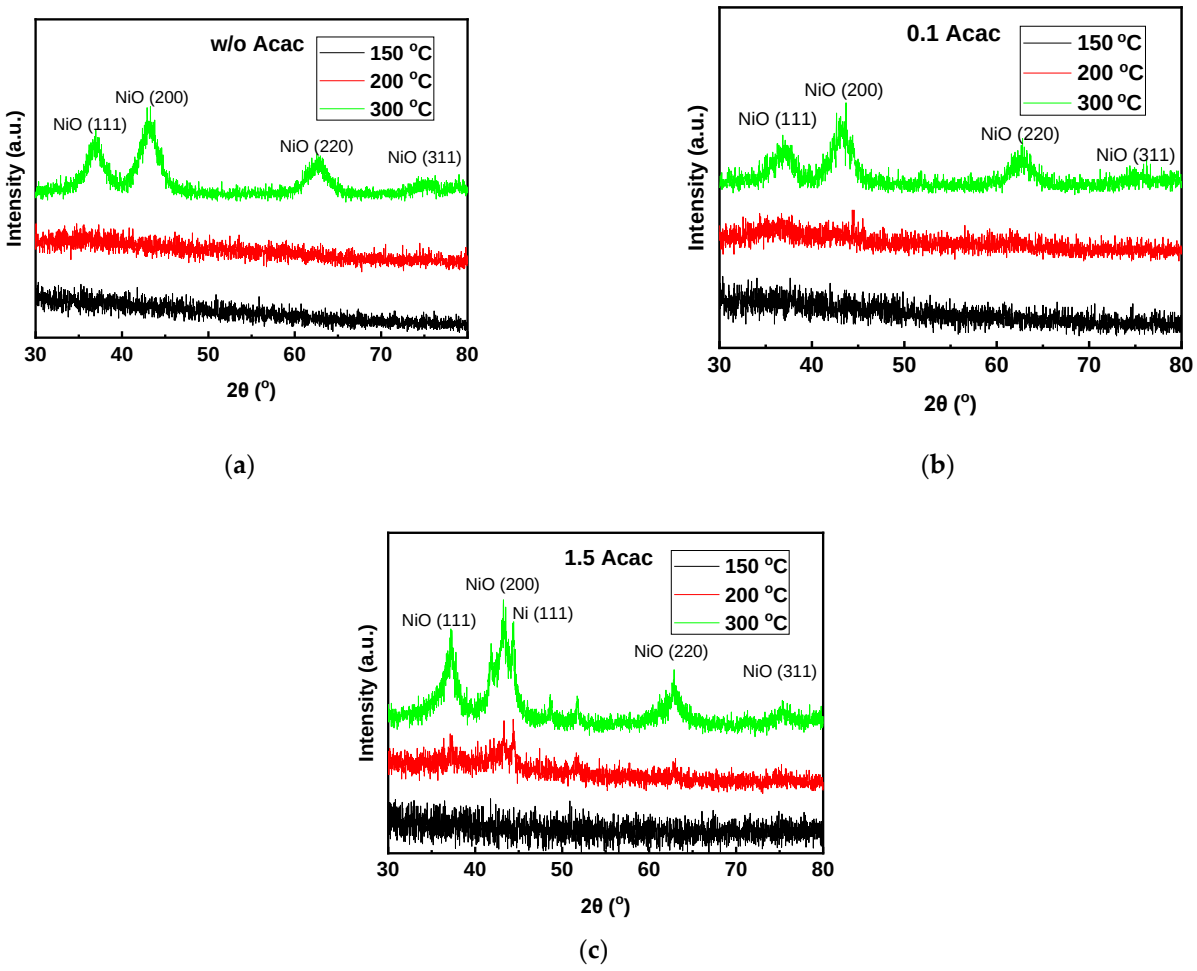

Figure 4. XRD patterns of the combustion synthesis of precursor films containing (**a**) w/o fuel (Acac), (**b**) 0.1, and (**c**) 1.5 molar ratio of fuel (Acac) to oxidizer (Cu, Ni nitrates) annealed at 150, 200, and 300 °C.

The crystallinity of the as-prepared materials obtained by combustion reaction of the bulk precursors was also examined using XRD analysis (Figure 5). Specifically, different initial molar ratios of the fuel to oxidizer (w/o, 0.1, and 1.5 Acac) at 200 °C annealing temperature of the bulk precursors were compared. The XRD results show a significant improvement in the crystallinity of the bulk Cu:NiO_x compared to the corresponding thin films. Moreover, the required annealing temperature for the crystal phase formation is significantly reduced (as was also evidenced by TGA analysis) when using the solution combustion synthesis of bulk materials as compared to the thin films. In the case of samples synthesized by bulk precursors, mixed crystal phases of metallic Ni (dominant species) and metal oxide NiO (residual species) were obtained regardless of the molar ratio of fuel to oxidizer precursors. Specifically, XRD patterns revealed that intense peaks appeared

at 44.0°, 52.3°, and 76.5° assigned to the (111), (200), and (220) planes, respectively, of face-centered cubic Ni (JCPDS No. 87-0712) (main product). The presence of Ni phase is an indication of combustion with a rich fuel precursor; therefore, even in the precursor w/o Acac, the Ni phase is the main product implying that, again, 2-methoxy ethanol plays a dual role of acting both as a solvent and a fuel [26]. The high crystallinity of bulk materials, as evidenced by the sharper diffractions in XRD patterns, is attributed to the release of high energy in the exothermic reaction that occurred by solution combustion synthesis (SCS). Thus, in agreement with the findings from TGA measurements, the complete combustion occurs mainly due to the bulk precursor material, which has a higher mass compared to corresponding films [55].

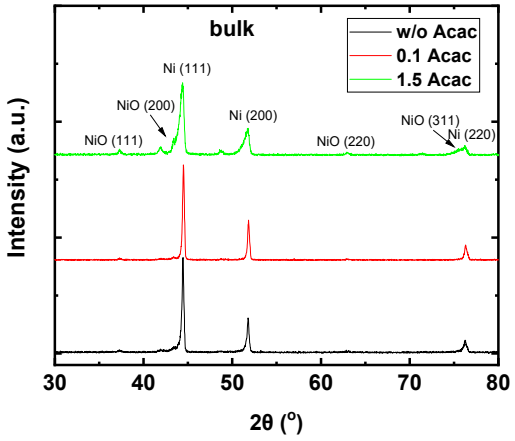

Figure 5. XRD patterns of combustion-synthesized samples (bulk) prepared from precursors containing w/o, 0.1, and 1.5 molar ratio of fuel (Acac) to oxidizer (Cu, Ni nitrates) annealed at 200 °C.

3.3. Cu:NiO_x Thin Films Characterization

X-ray photoelectron spectroscopy (XPS) was employed to investigate the chemical state of the Cu:NiO_x surface. The XPS survey scans of the Cu:NiO_x films synthesized with 0.1 Acac and annealed at 200 and 300 °C evidenced the presence of Ni, Cu, O, and C elements (see Supplementary Figure S1). In the Cu:NiO_x film annealed at 200 °C, the N1s spectrum indicated the presence of some reduced nitrogen (399.8 eV), NiO_2^- (403.6 eV) and NiO_3^- (406.8 eV) containing species (Figure 6a), while the N1s scan of the 300 °C annealed film showed the existence of reduced nitrogen (399.0) and NO_x (405.6 eV) residues (Figure 6b) [59]. For the film annealed at 200 °C, the spectrum of the Ni 2p region (Figure 6c) showed a double peak at 856.3 eV (Ni $2p_{3/2}$) and 874.0 eV (Ni $2p_{1/2}$) binding energies, accompanied by shake-up satellite peaks at 862.0 eV and 879.7 eV, which are characteristic of Ni^{2+}–oxygen bonded complexes, possibly in the form of $Ni(acac)_2$ [60], while the XPS Ni 2p spectrum of the 300 °C annealed film (Figure 6d) indicated the presence of NiO, showing a characteristic double peak at 854.6 eV (Ni $2p_{3/2}$) and 872.3 eV (Ni $2p_{1/2}$) binding energies (spin-orbit splitting of 17.7 eV) along with shake-up satellite peaks at 861.2 and 878.8 eV [61]. Furthermore, the XPS Cu 2p spectrum of the 300 °C annealed film (Figure 6e) exhibited a double peak at 934.2 eV and 953.9 eV due to the Cu $2p_{3/2}$ and Cu $2p_{1/2}$ core level components of the CuO (Cu $2p_{3/2}$: 934.7 eV and Cu $2p_{3/2}$: 954.5 eV for the 200 °C annealed film, Figure 6f), consistent with other reports [62,63]. As for the broad signals located at 940.6 and 953.9 eV (943.0 eV for the 200 °C annealed film), they are assigned to the shake-up satellite peaks of paramagnetic Cu^{2+}. The incorporation of Cu^{2+} ions into the NiO lattice was also verified by the Auger α parameter, that is, the kinetic energy of the Cu $L_3M_{4,5}M_{4,5}$ Auger peak plus binding energy of the Cu $2p_{3/2}$ peak. For the 300 °C annealed film, the Auger parameter was calculated to be 1851.8 eV, which respects the existing phase of CuO [64]. Quantitative analysis from the XPS spectra also indicated that the film that annealed at 200 °C contained 6.51 wt.% CH_xO_y and 3.32 wt.%, with NO_x containing organic compounds, while the corresponding remnants for the 300

°C annealed film was found to be 0.64 wt.% and 0.33%, respectively (see Supplementary Table S1). The higher amount of remnants found in 200 °C annealed film suggests the incomplete combustion reaction of Cu:NiO_x precursors, in agreement with the TGA results (Figure 2). Moreover, the Cu atomic concentration (Cu doping level) in the Cu:NiO_x films annealed at 200 and 300 °C was found to be 5.64% and 5.84%, respectively, which is very close to the nominal composition.

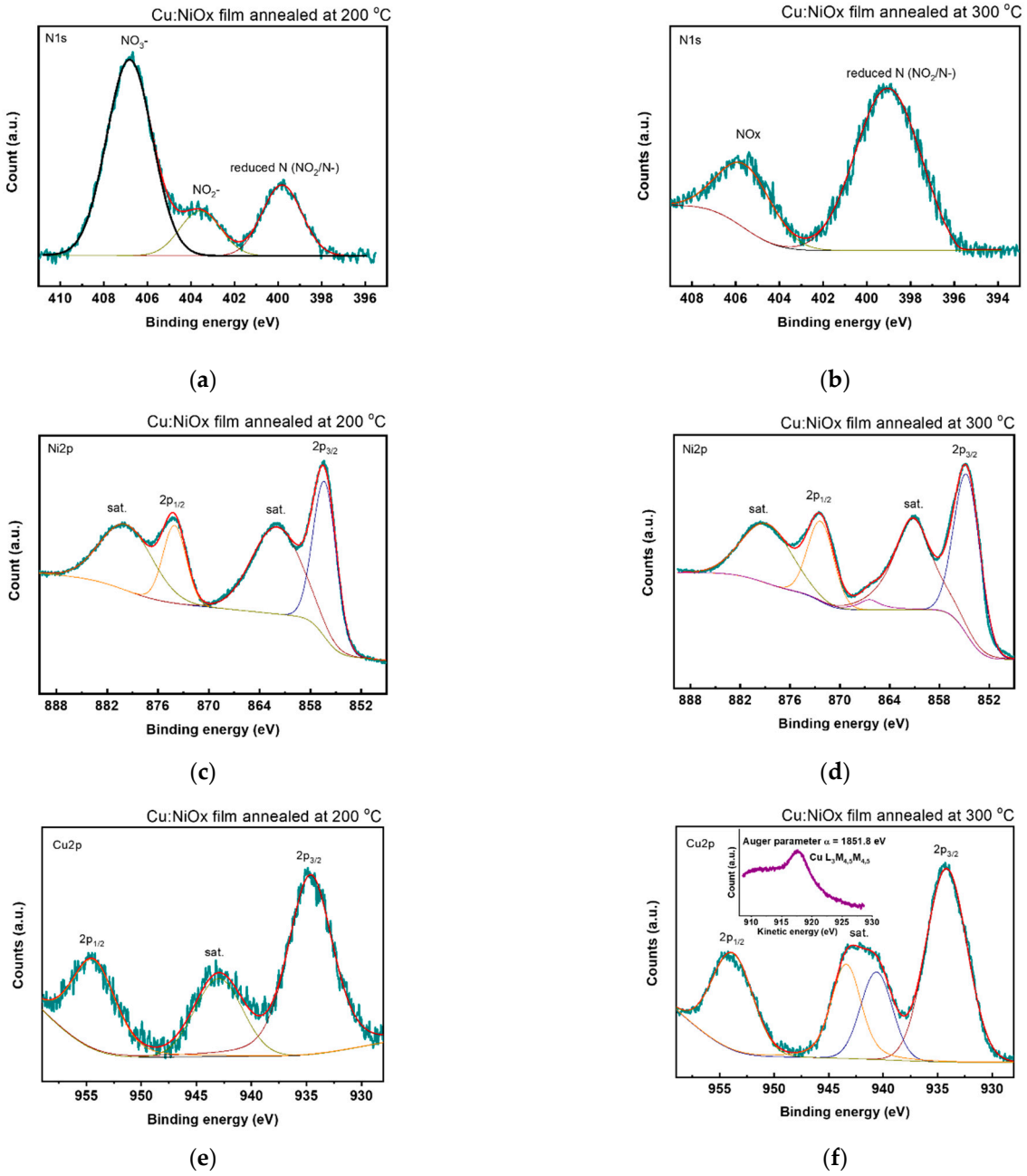

Figure 6. XPS spectra of the (**a**,**b**) N 1s, (**c**,**d**) Ni 2p and (**e**,**f**) Cu 2p region of the Cu:NiO_x films fabricated from precursor containing 0.1 Acac and annealed at 200 °C and 300 °C. Inset of panel (**f**): the Cu $L_3M_{4,5}M_{4,5}$ Auger XPS spectrum.

Furthermore, we examined the film topography of Cu:NiO_x films fabricated on quartz substrates by contact angle and UV-Vis spectroscopy. Figure 7 shows the film morphology using AFM for the films synthesized from precursors containing 0.1 Acac and annealed at 150 and 300 °C, respectively. It is clearly observed that the film treated at 150 °C shows a featured structure of large particles, due to the presence of residues, with a surface roughness of 1.5 nm (Figure 7a). On the other hand, the film treated at 300 °C does not

show structured features due to the small size of the Cu:NiO_x particles, exhibiting a surface roughness of 0.7 nm (Figure 7b). The final thickness of the film annealed at 150 and 300 °C is ~80 and ~50 nm, respectively, due to the considerable amount of residue that remained in the 150 °C annealed film, as shown above through XPS analysis for films synthesized at low annealing temperatures.

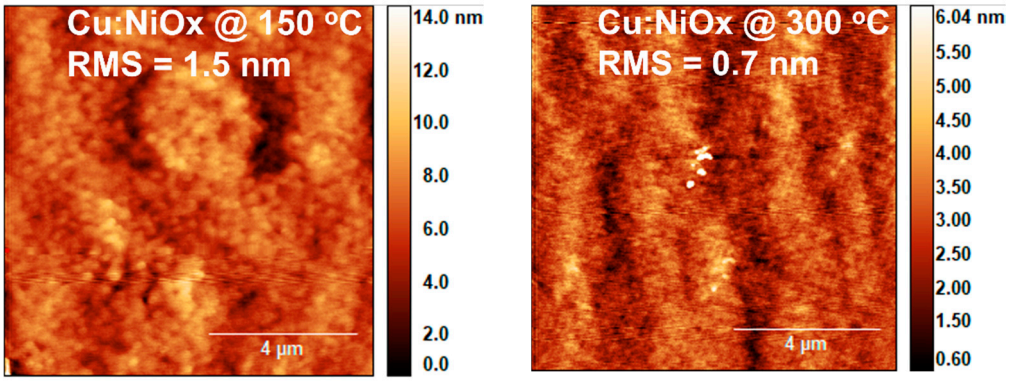

(**a**) (**b**)

Figure 7. AFM images of Cu:NiO_x films fabricated on quartz substrates from precursor containing 0.1 molar ratio of fuel (Acac) to oxidizer (Cu, Ni nitrates) annealed at (**a**) 150 and (**b**) 300 °C.

The UV-vis absorption spectrum (Figure 8) of the films treated at 150 and 200 °C show no prominent absorption due to the amorphous nature of metal oxides, while, for 300 °C annealing film, the absorption onset at ~400 nm (~3.1 eV) and strong absorption at ~350 nm (~3.5 eV) is ascribed to the crystalline Cu:NiO_x phase.

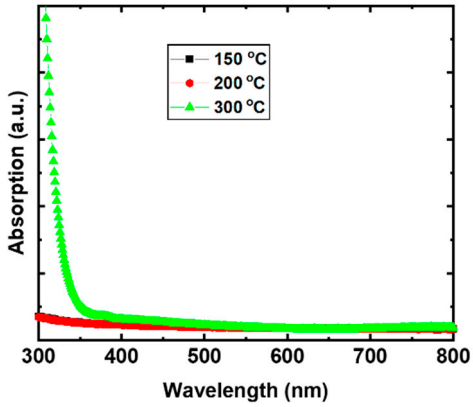

Figure 8. UV-Vis absorption of Cu:NiO_x films fabricated on quartz substrates from precursor containing 0.1 molar ratio of fuel (Acac) to oxidizer (Cu, Ni nitrates) annealed at 150, 200, and 300 °C.

The contact angle of water was measured on films annealed at 150, 170, and 200 °C, using a fuel to oxidizer ratio of 0 (w/o), 0.1, and 1.5 (see Supplementary Figure S2), from which the measured values are plotted in Figure 9. All the contact angles are higher than 60°, irrespective of fuel concentration, in contrast to the contact angle of the Cu:NiO_x film (0.1 molar ratio of Acac to oxidizer) annealed at 300 °C, which is substantially lower (20°); see Supplementary Figure S3. Thus, we infer that the remnants (see XPS analysis) in the low temperature treated film form a Cu:NiO_x surface with moderate wettability, while the films annealed at 300 °C, where the surface is almost free from remnants, show an improved wettability.

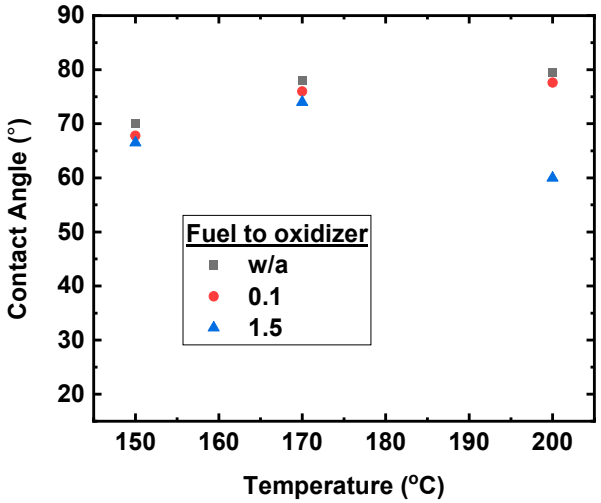

Figure 9. A graph presenting the contact angles of water on films prepared using precursor containing w/o Acac, 0.1, and 1.5 molar ratio of fuel (Acac) to oxidizer (Cu, Ni nitrates) annealed at 150, 170, and 200 °C.

3.4. J-V Characterization of Cu:NiO$_x$ Films as HTLs in Planar p-i-n PVSCs

To evaluate the functionality of the different Cu:NiO$_x$ films as HTLs in solar cells, 50 nm thick Cu:NiO$_x$ films, synthesized using the previously described conditions, were implemented in inverted perovskite solar cells with structure ITO/Cu:NiO$_x$/perovskite/PC$_{60}$BM/BCP/Ag and the J-V device characteristics under 1 sun simulated light were recorded.

As it is presented in J–V curves of Figure 10a, the devices that incorporated Cu:NiO$_x$ films annealed at 150 °C and 200 °C exhibited a very limited functionality. All the devices show low V_{oc} in the range of 0.3 V, and the generated current is below 1 mA/cm^2. The device with a 1.5 molar ratio Acac to oxidizer that was annealed at 200 °C shows an almost linear response of the current density to the sweeping voltage, which can be attributed to partially formed metallic Ni, as can be inferred by the corresponding XRD results in Figure 4c. In contrast, the inverted perovskite solar cells which incorporate Cu:NiO$_x$ HTLs prepared from precursor solutions containing w/o, 0.1, and 1.5 Acac annealed at 300 °C, delivered higher efficiency. In Figure 10b, the J–V curves of the best performing devices under 1 sun simulated light are illustrated, and the extracted solar cell parameters of the studied devices are presented in Table 1—the average values of 12 devices for each batch are indicated in brackets. Regarding the impact of the fuel to oxidizer ratio on the devices' PCE, the devices with Cu:NiO$_x$ HTL where the precursor contained no fuel (w/o Acac) and a 0.1 Acac ratio showed similar PCE values, and the devices which incorporated Cu:NiO$_x$ film synthesized with 1.5 Acac/oxidizer ratio showed a reduced V_{oc} and J_{sc} efficiency, resulting in lower PCE.

The experimental results presented within this manuscript using a triple cation $Cs_{0.04}(MA_{0.17}FA_{0.83})_{0.96}$ $Pb(I_{0.83}Br_{0.17})_3$ perovskite formulation infer that the Cu:NiO$_x$ oxide's precursor films that were annealed at temperatures of 150 and 200 °C produce electronic films that cannot function as HTLs for efficient inverted perovskite solar cells. This is ascribed to the incomplete combustion that results in amorphous Cu:NiO$_x$ films with remnants. This result is in agreement with a previous report, where amorphous NiO$_x$ showed limited functionality as HTL when applied in organic solar cells [65]. On the other hand, as shown above, the pure crystalline phase of Cu:NiO$_x$ HTL was obtained by annealing at 300 °C for the precursors w/o and with a 0.1 ratio of Acac/oxidizer, whereas, for the 1.5 ratio, metallic Ni are likely to be present within Cu:NiO$_x$ films (as indicated within the XRD pattern in Figure 4c). The pure crystalline phases (w/o and 0.1 ratio Acac/oxidizer) of Cu:NiO$_x$ resulted to better PCEs 15.97% (average 14.48%) and 16.58% (average 14.85%), respectively, while, for the 1.5 ratio, the metallic Ni influence delivers lower PCE devices 14.90% (average 13.50%).

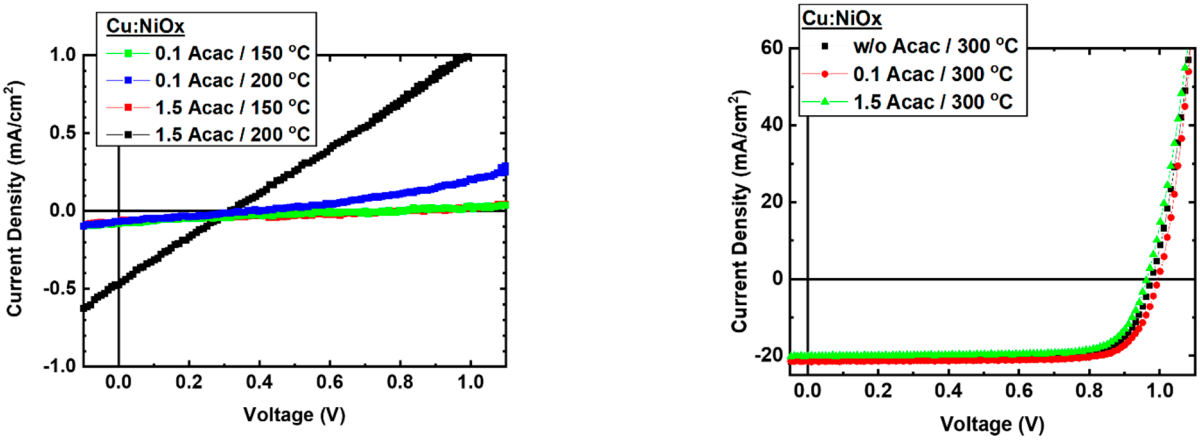

Figure 10. J–V curves of ITO/Cu:NiO_x/perovskite/$PC_{60}BM$/BCP/Ag devices under 1 sun simulated light for Cu:NiO_x films fabricated from precursor containing (**a**) 0.1 and 1.5 molar ratio of fuel (Acac) to oxidizer (Cu, Ni nitrates) annealed at 150 and 200 °C, and from precursor containing (**b**) w/o Acac, 0.1, and 1.5 molar ratio of fuel (Acac) to oxidizer (Cu, Ni nitrates) annealed at 300 °C.

Table 1. Extracted solar cell parameters of the best ITO/Cu:NiO_x/perovskite/$PC_{60}BM$/BCP/Ag devices. The average values of 12 devices for each batch are shown in brackets.

Sample	V_{oc} (V)	J_{sc} (mA/cm^2)	FF (%)	PCE (%)
w/o Acac	0.98 (0.97)	21.11 (20.64)	77.1 (72.3)	15.97 (14.48)
0.1 Acac	0.99 (0.97)	21.40 (20.75)	78.2 (73.8)	16.58 (14.85)
1.5 Acac	0.96 (0.94)	20.03 (19.64)	77.3 (73.1)	14.90 (13.50)

4. Discussion

In this work, we examined the solution combustion synthesis of Cu:NiO_x films by using different molar ratios (w/o, 0.1, and 1.5) of fuel acetylacetone (Acac) to oxidizer (nitrates) precursors as well as various thermal processing annealing temperatures (150, 200, and 300 °C). Thermogravimetric analysis (TGA and DTA) results showed that the complete combustion process at ~150 °C can occur in bulk analogues. XRD measurements revealed that the corresponding Cu:NiO_x films crystallize to NiO phase upon annealing temperature at 300 °C irrespective of Acac concentration, while, for lower annealing temperatures (150, 200 °C), no crystal phase was observed. XPS, AFM, UV-Vis spectroscopy, and contact angle measurements on the films strongly support the incomplete combustion of the Cu:NiO_x thin films for annealing temperatures at 150 °C and 200 °C. XPS measurements of the Cu:NiO_x film revealed the presence of a high atomic ratio of remnants for thermal annealing at 200 °C, which are remarkably reduced for films annealed at 300 °C. Surface topography images and thickness measurements via AFM and profilometer showed that the Cu:NiO_x films annealed at 300 °C have a lower thickness (~50 nm) and roughness (~0.7 nm) compared to ~80 nm thickness and ~1.5 nm roughness for the Cu:NiO_x films annealed at temperatures 150 °C due to remnants in the film. Moreover, Cu:NiO_x films annealed at 300 °C have an improved hydrophilicity, showing a contact angle of 20°, while the films annealed at 150 °C and 200 °C show angles of more than 60° due to surface remnants. Regarding the optical absorption measurements, the 300 °C thermally annealed films exhibit a distinct absorption curve ascribed to the formed crystalline Cu:NiO_x, while the lower annealing temperature films at 150 °C and 200 °C lack any strong absorption in the range of measured wavelengths due to the amorphous phase; these results are consistent with the paper reported in the XRD findings. To conclude, the presented solution combustion chemistry findings in Cu:NiO_x thin films are confirmed by applying the various ratios of Acac/Oxidizer and annealing processing temperatures of SCS-based Cu:NiO_x HTLs in triple cation-based $Cs_{0.04}(MA_{0.17}FA_{0.83})_{0.96}$ $Pb(I_{0.83}Br_{0.17})_3$ inverted PVSCs. The

Cu:NiO_x HTLs annealed at temperatures 150 °C and 200 °C, irrespective of Acac/Oxidizer ratios, provided limited functionality in the PVSCs due to incomplete an combustion process that resulted in amorphous Cu:NiO_x with remnants, as confirmed by the presented XRD and XPS measurements, respectively. The crystalline phase of Cu:NiO_x HTLs and efficient inverted PVSCs performance obtained at an annealing temperature of 300 °C irrespective of the Acac/Oxidizer ratio. Following the solution combustion synthesis route that has been investigated within this manuscript, the Cu:NiO_x crystalline HTLs annealed at 300 °C, with a 0.1 ratio of Acac/oxidizer resulting in 16.58% PCE for the triple cation-based $Cs_{0.04}(MA_{0.17}FA_{0.83})_{0.96}$ $Pb(I_{0.83}Br_{0.17})_3$ inverted PVSCs.

Supplementary Materials: The following are available online at https://www.mdpi.com/article/10.3390/nano11113074/s1, Figure S1: XPS survey spectra of the Cu:NiO_x films fabricated from precursor containing 0.1 Acac and annealed at (a) 200 °C and (b) 300 °C; Table S1: XPS calculated atomic ratios for the Cu:NiO_x films fabricated form precursor containing 0.1 Acac and annealed at 200 and 300 °C; Figure S2: contact angle picture of water on films prepared using precursor containing w/o, 0.1, and 1.5 molar ratio of fuel (Acac) to oxidizer (Cu, Ni nitrates) annealed at 150, 170, and 200 °C; Figure S3: contact angle picture of water on films prepared using precursor 0.1 molar ratio of fuel (Acac) to oxidizer (Cu, Ni nitrates) annealed at 300 °C showing an angle of 20°.

Author Contributions: Conceptualization, A.I., I.T.P. and S.A.C.; Data curation, A.I., I.T.P., G.S.A. and E.D.K.; Formal analysis, A.I., I.T.P., E.D.K., G.S.A. and S.A.C.; Investigation, A.I., I.T.P., G.S.A. and S.A.C.; Methodology, A.I., I.T.P. and S.A.C.; Supervision, G.S.A. and S.A.C.; Funding acquisition, S.A.C.; Writing—original draft, A.I., I.T.P. and S.A.C.; Writing—review and editing, G.S.A. and S.A.C. All authors have read and agreed to the published version of the manuscript.

Funding: This research was funded by the European Research Council (ERC) under the European Union's Horizon 2020 research and innovation program, (H2020 European Research Council, grant number 647311), and further supported from the academic yearly research activity internal Cyprus University of Technology budget.

Conflicts of Interest: The authors declare no conflict of interest.

References

1. Kojima, A.; Teshima, K.; Shirai, Y.; Miyasaka, T. Organometal Halide Perovskites as Visible-Light Sensitizers for Photovoltaic Cells. *J. Am. Chem. Soc.* **2009**, *131*, 6050–6051. [CrossRef]
2. Jeong, M.; Choi, I.W.; Go, E.M.; Cho, Y.; Kim, M.; Lee, B.; Jeong, S.; Jo, Y.; Choi, H.W.; Lee, J.; et al. Stable perovskite solar cells with efficiency exceeding 24.8% and 0.3-V voltage loss. *Science* **2020**, *369*, 1615LP–1620LP. [CrossRef]
3. Huang, A.B.; Zhu, J.T.; Zheng, J.Y.; Yu, Y.; Liu, Y.; Yang, S.W.; Bao, S.H.; Lei, L.; Jin, P. Achieving high-performance planar perovskite solar cells with co-sputtered Co-doping NiO_x hole transport layers by efficient extraction and enhanced mobility. *J. Mater. Chem. C* **2016**, *4*, 10839–10846. [CrossRef]
4. Seo, S.; Park, I.J.; Kim, M.; Lee, S.; Bae, C.; Jung, H.S.; Park, N.; Kim, J.Y.; Shin, H. An ultra-thin, un-doped NiO hole transporting layer of highly efficient (16.4%) organic–inorganic hybrid perovskite solar cells. *Nanoscale* **2016**, *8*, 11403–11412. [CrossRef]
5. Singh, C.C.; Roy Choudhury, A.N.; Sutar, D.S.; Sarkar, S.K. Plasma-assisted combustion synthesis of p -type transparent Cu incorporated NiO thin films-Correlation between deposition chemistry and charge transport characteristics. *J. Appl. Phys.* **2021**, *129*. [CrossRef]
6. Hietzschold, S.; Hillebrandt, S.; Ullrich, F.; Bombsch, J.; Rohnacher, V.; Ma, S.; Liu, W.; Köhn, A.; Jaegermann, W.; Pucci, A.; et al. Functionalized Nickel Oxide Hole Contact Layers: Work Function versus Conductivity. *ACS Appl. Mater. Interfaces* **2017**, *9*, 39821–39829. [CrossRef]
7. Abdy, H.; Aletayeb, A.; Kolahdouz, M.; Soleimani, E.A. Investigation of metal-nickel oxide contacts used for perovskite solar cell. *AIP Adv.* **2019**, *9*, 015216. [CrossRef]
8. Wei, Y.; Yao, K.; Wang, X.; Jiang, Y.; Liu, X.; Zhou, N.; Li, F. Improving the efficiency and environmental stability of inverted planar perovskite solar cells via silver-doped nickel oxide hole-transporting layer. *Appl. Surf. Sci.* **2018**, *427*, 782–790. [CrossRef]
9. Li, G.; Jiang, Y.; Deng, S.; Tam, A.; Xu, P.; Wong, M.; Kwok, H.-S. Overcoming the Limitations of Sputtered Nickel Oxide for High-Efficiency and Large-Area Perovskite Solar Cells. *Adv. Sci.* **2017**, *4*, 1700463. [CrossRef]
10. Liu, M.-H.; Zhou, Z.-J.; Zhang, P.-P.; Tian, Q.-W.; Zhou, W.-H.; Kou, D.-X.; Wu, S.-X. p-type Li, Cu-codoped NiO_x hole-transporting layer for efficient planar perovskite solar cells. *Opt. Express* **2016**, *24*, A1349. [CrossRef]
11. Tang, L.J.; Chen, X.; Wen, T.Y.; Yang, S.; Zhao, J.J.; Qiao, H.W.; Hou, Y.; Yang, H.G. A Solution-Processed Transparent NiO Hole-Extraction Layer for High-Performance Inverted Perovskite Solar Cells. *Chem. A Eur. J.* **2018**, *24*, 2845–2849. [CrossRef] [PubMed]

12. He, C.; Zhang, F.; Zhao, X.; Lin, C.; Ye, M. Interface engineering of BCP buffer layers in planar heterojunction perovskite solar cells with NiO_x hole transporting layers. *Front. Phys.* **2018**, *6*, 1–6. [CrossRef]
13. Chen, W.; Liu, F.-Z.; Feng, X.-Y.; Djurišić, A.B.; Chan, W.K.; He, Z.-B. Cesium Doped NiO_x as an Efficient Hole Extraction Layer for Inverted Planar Perovskite Solar Cells. *Adv. Energy Mater.* **2017**, *7*, 1700722. [CrossRef]
14. Di Girolamo, D.; Matteocci, F.; Kosasih, F.U.; Chistiakova, G.; Zuo, W.; Divitini, G.; Korte, L.; Ducati, C.; Di Carlo, A.; Dini, D.; et al. Stability and Dark Hysteresis Correlate in NiO-Based Perovskite Solar Cells. *Adv. Energy Mater.* **2019**, *9*, 1–10. [CrossRef]
15. Qiu, Z.; Gong, H.; Zheng, G.; Yuan, S.; Zhang, H.; Zhu, X.; Zhou, H.; Cao, B. Enhanced physical properties of pulsed laser deposited NiO films via annealing and lithium doping for improving perovskite solar cell efficiency. *J. Mater. Chem. C* **2017**, *5*, 7084–7094. [CrossRef]
16. Nishihara, Y.; Chikamatsu, M.; Kazaoui, S.; Miyadera, T.; Yoshida, Y. Influence of O_2 plasma treatment on NiO x layer in perovskite solar cells. *Jpn. J. Appl. Phys.* **2018**, *57*, 04FS07. [CrossRef]
17. Kim, J.H.; Liang, P.W.; Williams, S.T.; Cho, N.; Chueh, C.C.; Glaz, M.S.; Ginger, D.S.; Jen, A.K.Y. High-performance and environmentally stable planar heterojunction perovskite solar cells based on a solution-processed copper-doped nickel oxide hole-transporting layer. *Adv. Mater.* **2015**, *27*, 695–701. [CrossRef]
18. Chen, W.; Wu, Y.; Fan, J.; Djurišić, A.B.; Liu, F.; Tam, H.W.; Ng, A.; Surya, C.; Chan, W.K.; Wang, D.; et al. Understanding the Doping Effect on NiO: Toward High-Performance Inverted Perovskite Solar Cells. *Adv. Energy Mater.* **2018**, *8*, 1703519. [CrossRef]
19. Kim, H.-S.; Seo, J.-Y.; Park, N.-G. Impact of Selective Contacts on Long-Term Stability of $CH_3NH_3PbI_3$ Perovskite Solar Cells. *J. Phys. Chem. C* **2016**, *120*, 27840–27848. [CrossRef]
20. Wang, H.; Zeng, X.; Huang, Z.; Zhang, W.; Qiao, X.; Hu, B.; Zou, X.; Wang, M.; Cheng, Y.-B.; Chen, W. Boosting the Photocurrent Density of p-Type Solar Cells Based on Organometal Halide Perovskite-Sensitized Mesoporous NiO Photocathodes. *ACS Appl. Mater. Interfaces* **2014**, *6*, 12609–12617. [CrossRef]
21. Chen, W.; Wu, Y.; Yue, Y.; Liu, J.; Zhang, W.; Yang, X.; Chen, H.; Bi, E.; Ashraful, I.; Grätzel, M.; et al. Efficient and stable large-area perovskite solar cells with inorganic charge extraction layers. *Science* **2015**, *350*, 944LP–948LP. [CrossRef]
22. Hu, L.; Peng, J.; Wang, W.; Xia, Z.; Yuan, J.; Lu, J.; Huang, X.; Ma, W.; Song, H.; Chen, W.; et al. Sequential Deposition of CH3NH3PbI3 on Planar NiO Film for Efficient Planar Perovskite Solar Cells. *ACS Photonics* **2014**, *1*, 547–553. [CrossRef]
23. Kim, M.G.; Kanatzidis, M.G.; Facchetti, A.; Marks, T.J. Low-temperature fabrication of high-performance metal oxide thin-film electronics via combustion processing. *Nat. Mater.* **2011**, *10*, 382–388. [CrossRef] [PubMed]
24. Branquinho, R.; Santa, A.; Carlos, E.; Salgueiro, D.; Barquinha, P.; Martins, R.; Fortunato, E. Solution Combustion Synthesis: Applications in Oxide Electronics. In *Developments in Combustion Technology*; InTechOpen Ltd.: London, UK, 2016.
25. Hennek, J.W.; Smith, J.; Yan, A.; Kim, M.G.; Zhao, W.; Dravid, V.P.; Facchetti, A.; Marks, T.J. Oxygen "getter" effects on microstructure and carrier transport in low temperature combustion-processed a-InXZnO (X = Ga, Sc, Y, La) transistors. *J. Am. Chem. Soc.* **2013**, *135*, 10729–10741. [CrossRef]
26. Varma, A.; Mukasyan, A.S.; Rogachev, A.S.; Manukyan, K.V. Solution Combustion Synthesis of Nanoscale Materials. *Chem. Rev.* **2016**, *116*, 14493–14586. [CrossRef]
27. Li, J.; Han, X.; Zhao, Y.; Li, J.; Wang, M.; Dong, C. Solar Energy Materials and Solar Cells One–step synthesis of Cu 3 BiS 3 thin fi lms by a dimethyl sulfoxide (DMSO)–based solution coating process for solar cell application. *Sol. Energy Mater. Sol. Cells* **2018**, *174*, 593–598. [CrossRef]
28. Wang, J.; Daunis, T.B.; Cheng, L.; Zhang, B.; Kim, J.; Hsu, J.W.P. Combustion Synthesis of p-Type Transparent Conducting $CuCrO_{2+x}$ and Cu:CrO_x Thin Films at 180 °C. *ACS Appl. Mater. Interfaces* **2018**, *10*, 3732–3738. [CrossRef]
29. Bolaghi, Z.K.; Hasheminiasari, M.; Masoudpanah, S.M. Solution combustion synthesis of ZnO powders using mixture of fuels in closed system. *Ceram. Int.* **2018**, *44*, 12684–12690. [CrossRef]
30. Zheng, D.; Wang, G.; Huang, W.; Wang, B.; Ke, W.; Logsdon, J.L.; Wang, H.; Wang, Z.; Zhu, W.; Yu, J.; et al. Combustion Synthesized Zinc Oxide Electron-Transport Layers for Efficient and Stable Perovskite Solar Cells. *Adv. Funct. Mater.* **2019**, *29*, 1–10. [CrossRef]
31. Ullaha, S.; De Matteis, F.; Tor, R.; Politecnico, V.; Martins, R.; Branquinho, R.; Fortunato, E.; Davoli, I.; Fisica, D.; Tor, R. A Combination of Solution Synthesis & Solution Combustion Synthesis for Highly Conducting and Transparent Aluminum Zinc Oxide Thin Films. In Proceedings of the 2015 IEEE 15th International Conference on Nanotechnology (IEEE-NANO), Rome, Italy, 27–30 July 2015; pp. 144–147. [CrossRef]
32. Xu, C.; Manukyan, K.V.; Adams, R.A.; Pol, V.G.; Chen, P.; Varma, A. One-step solution combustion synthesis of $CuO/Cu_2O/C$ anode for long cycle life Li-ion batteries. *Carbon* **2019**, *142*, 51–59. [CrossRef]
33. Zhang, J.; Zhang, M.; Lin, L.; Wang, X. Sol Processing of Conjugated Carbon Nitride Powders for Thin-Film Fabrication. *Angew. Chem.* **2015**, *127*, 6395–6399. [CrossRef]
34. Everaerts, K.; Zeng, L.; Hennek, J.W.; Camacho, D.I.; Jariwala, D.; Bedzyk, M.J.; Hersam, M.C.; Marks, T.J. Printed indium gallium zinc oxide transistors. Self-assembled nanodielectric effects on low-temperature combustion growth and carrier mobility. *ACS Appl. Mater. Interfaces* **2013**, *5*, 11884–11893. [CrossRef]
35. Di Girolamo, D.; Matteocci, F.; Lamanna, E.; Calabrò, E.; Di Carlo, A.; Dini, D. Inverted perovskite solar cells with transparent hole transporting layer based on semiconducting nickel oxide. In Proceedings of the AIP Conference Proceedings, Rome, Italy, 26–29 September 2017; American Institute of Physics Inc.: Melville, NY, USA, 2018; Volume 1990.

36. Sanctis, S.; Hoffmann, R.C.; Koslowski, N.; Foro, S.; Bruns, M.; Schneider, J.J. Aqueous Solution Processing of Combustible Precursor Compounds into Amorphous Indium Gallium Zinc Oxide (IGZO) Semiconductors for Thin Film Transistor Applications. *Chem. Asian J.* **2018**, *13*, 3912–3919. [CrossRef]
37. Chen, Y.; Wang, B.; Huang, W.; Zhang, X.; Wang, G.; Leonardi, M.J.; Huang, Y.; Lu, Z.; Marks, T.J.; Facchetti, A. Nitroacetylacetone as a Cofuel for the Combustion Synthesis of High-Performance Indium-Gallium-Zinc Oxide Transistors. *Chem. Mater.* **2018**, *30*, 3323–3329. [CrossRef]
38. Papadas, I.T.; Ioakeimidis, A.; Armatas, G.S.; Choulis, S.A. Low-Temperature Combustion Synthesis of a Spinel $NiCo_2O_4$ Hole Transport Layer for Perovskite Photovoltaics. *Adv. Sci.* **2018**, *5*, 1701029. [CrossRef] [PubMed]
39. Ioakeimidis, A.; Papadas, I.T.; Tsikritzis, D.; Armatas, G.S.; Kennou, S.; Choulis, S.A. Enhanced photovoltaic performance of perovskite solar cells by Co-doped spinel nickel cobaltite hole transporting layer. *APL Mater.* **2019**, *7*, 021101. [CrossRef]
40. Galatopoulos, F.; Papadas, I.T.; Ioakeimidis, A.; Eleftheriou, P.; Choulis, S.A. Surface treatment of cu:Nio_x hole-transporting layer using β-alanine for hysteresis-free and thermally stable inverted perovskite solar cells. *Nanomaterials* **2020**, *10*, 1961. [CrossRef] [PubMed]
41. Ioakeimidis, A.; Choulis, S.A. Nitrobenzene as additive to improve reproducibility and degradation resistance of highly efficient methylammonium-free inverted Perovskite solar cells. *Materials* **2020**, *13*, 3289. [CrossRef]
42. Jung, J.W.; Chueh, C.C.; Jen, A.K.Y. A Low-Temperature, Solution-Processable, Cu-Doped Nickel Oxide Hole-Transporting Layer via the Combustion Method for High-Performance Thin-Film Perovskite Solar Cells. *Adv. Mater.* **2015**, *27*, 7874–7880. [CrossRef]
43. Han, W.; Ren, G.; Li, Z.; Dong, M.; Liu, C.; Guo, W. Improving the performance of perovskite solar cells by surface passivation. *J. Energy Chem.* **2020**, *46*, 202–207. [CrossRef]
44. He, J.; Xiang, Y.; Zhang, F.; Lian, J.; Hu, R.; Zeng, P.; Song, J.; Qu, J. Improvement of red light harvesting ability and open circuit voltage of Cu:NiO_x based p-i-n planar perovskite solar cells boosted by cysteine enhanced interface contact. *Nano Energy* **2018**, *45*, 471–479. [CrossRef]
45. Kim, H.S.; Seo, J.Y.; Xie, H.; Lira-Cantu, M.; Zakeeruddin, S.M.; Gratzel, M.; Hagfeldt, A. Effect of cs-incorporated NiO_x on the performance of perovskite solar cells. *ACS Omega* **2017**, *2*, 9074–9079. [CrossRef] [PubMed]
46. Liu, Z.; Chang, J.; Lin, Z.; Zhou, L.; Yang, Z.; Chen, D.; Zhang, C.; Liu, S.; Hao, Y. High-Performance Planar Perovskite Solar Cells Using Low Temperature, Solution–Combustion-Based Nickel Oxide Hole Transporting Layer with Efficiency Exceeding 20%. *Adv. Energy Mater.* **2018**, *8*, 1–9. [CrossRef]
47. Thiruchelvan, P.S.; Lai, C.C.; Tsai, C.H. Combustion processed nickel oxide and zinc doped nickel oxide thin films as a hole transport layer for perovskite solar cells. *Coatings* **2021**, *11*, 627. [CrossRef]
48. Liu, Y.; Song, J.; Qin, Y.; Qiu, Q.; Zhao, Y.; Zhu, L.; Qiang, Y. Cu-doped nickel oxide hole transporting layer via efficient low-temperature spraying combustion method for perovskite solar cells. *J. Mater. Sci. Mater. Electron.* **2019**, *30*, 15627–15635. [CrossRef]
49. Liu, A.; Zhu, H.; Guo, Z.; Meng, Y.; Liu, G.; Fortunato, E.; Martins, R.; Shan, F. Solution Combustion Synthesis: Low-Temperature Processing for p-Type Cu:NiO Thin Films for Transparent Electronics. *Adv. Mater.* **2017**, *29*, 1–8. [CrossRef]
50. Li, Y.H.; Lu, X.; Wang, R.; Ma, Y.Y.; Duhm, S.; Fung, M.K. Cu-Doped nickel oxide prepared using a low-temperature combustion method as a hole-injection layer for high-performance OLEDs. *J. Mater. Chem. C* **2017**, *5*, 11751–11757. [CrossRef]
51. Cochran, E.A.; Park, D.H.; Kast, M.G.; Enman, L.J.; Perkins, C.K.; Mansergh, R.H.; Keszler, D.A.; Johnson, D.W.; Boettcher, S.W. Role of Combustion Chemistry in Low-Temperature Deposition of Metal Oxide Thin Films from Solution. *Chem. Mater.* **2017**, *29*, 9480–9488. [CrossRef]
52. Roura, P.; Farjas, J.; Eloussifi, H.; Carreras, L.; Ricart, S.; Puig, T.; Obradors, X. Thermal analysis of metal organic precursors for functional oxide preparation: Thin films versus powders. *Thermochim. Acta* **2015**, *601*, 1–8. [CrossRef]
53. Sánchez-Rodriguez, D.; Farjas, J.; Roura, P. The critical conditions for thermal explosion in a system heated at a constant rate. *Combust. Flame* **2017**, *186*, 211–219. [CrossRef]
54. Sánchez-Rodríguez, D.; Eloussifi, H.; Farjas, J.; Roura, P.; Dammak, M. Thermal gradients in thermal analysis experiments: Criterions to prevent inaccuracies when determining sample temperature and kinetic parameters. *Thermochim. Acta* **2014**, *589*, 37–46. [CrossRef]
55. Sanchez-Rodriguez, D.; Farjas, J.; Roura, P.; Ricart, S.; Mestres, N.; Obradors, X.; Puig, T. Thermal analysis for low temperature synthesis of oxide thin films from chemical solutions. *J. Phys. Chem. C* **2013**, *117*, 20133–20138. [CrossRef]
56. Cochran, E.A.; Woods, K.N.; Johnson, D.W.; Page, C.J.; Boettcher, S.W. Unique chemistries of metal-nitrate precursors to form metal-oxide thin films from solution: Materials for electronic and energy applications. *J. Mater. Chem. A* **2019**, *7*, 24124–24149. [CrossRef]
57. Saliba, M.; Correa-Baena, J.P.; Wolff, C.M.; Stolterfoht, M.; Phung, N.; Albrecht, S.; Neher, D.; Abate, A. How to Make over 20% Efficient Perovskite Solar Cells in Regular (n-i-p) and Inverted (p-i-n) Architectures. *Chem. Mater.* **2018**, *30*, 4193–4201. [CrossRef]
58. Salgueiro, D.; Kiazadeh, A.; Branquinho, R.; Santos, L.; Barquinha, P.; Martins, R.; Fortunato, E. Solution based zinc tin oxide TFTs: The dual role of the organic solvent. *J. Phys. D Appl. Phys.* **2017**, *50*. [CrossRef]
59. Nanayakkara, C.E.; Jayaweera, P.M.; Rubasinghege, G.; Baltrusaitis, J.; Grassian, V.H. Surface photochemistry of adsorbed nitrate: The role of adsorbed water in the formation of reduced nitrogen species on α-Fe_2O_3 particle surfaces. *J. Phys. Chem. A* **2014**, *118*, 158–166. [CrossRef]

60. de Souza, M.O.; Mendes, F.M.T.; de Souza, R.F.; dos Santos, J.H.Z. XPS characterization of nickel-acetylacetonate impregnated in NaX and NaY zeolites. *Microporous Mesoporous Mater.* **2004**, *69*, 217–221. [CrossRef]
61. Grosvenor, A.P.; Biesinger, M.C.; Smart, R.S.C.; McIntyre, N.S. New interpretations of XPS spectra of nickel metal and oxides. *Surf. Sci.* **2006**, *600*, 1771–1779. [CrossRef]
62. Islam, M.J.; Granollers Mesa, M.; Osatiashtiani, A.; Taylor, M.J.; Manayil, J.C.; Parlett, C.M.A.; Isaacs, M.A.; Kyriakou, G. The effect of metal precursor on copper phase dispersion and nanoparticle formation for the catalytic transformations of furfural. *Appl. Catal. B Environ.* **2020**, *273*, 119062. [CrossRef]
63. Wu, C.K.; Yin, M.; O'Brien, S.; Koberstein, J.T. Quantitative analysis of copper oxide nanoparticle composition and structure by X-ray photoelectron spectroscopy. *Chem. Mater.* **2006**, *18*, 6054–6058. [CrossRef]
64. Vasquez, R.P. CuO by XPS. *Surf. Sci. Spectra* **1998**, *5*, 262–266. [CrossRef]
65. Singh, A.; Gupta, S.K.; Garg, A. Inkjet printing of NiO films and integration as hole transporting layers in polymer solar cells. *Sci. Rep.* **2017**, *7*, 1–12. [CrossRef] [PubMed]